The density of ambient black carbon retrieved by a new method: implications to CCN prediction

Jingye Ren[1, 2], Fang Zhang[2*], Lu Chen[1], Jieyao Liu[1]

[1]*College of Global Change and Earth System Science, Beijing Normal University, Beijing 100875, China*

[2]*Shenzhen Key Laboratory of Organic Pollution Prevention and Control, School of Civil and Environmental Engineering, Harbin Institute of Technology (Shenzhen), 518055 Shenzhen, China*

Correspondence to: **Fang Zhang (zhangfang2021@hit.edu.cn)**

Abstract.

The effective density of black carbon (BC) is a crucial factor relevant to its aging degree that would add uncertainty in evaluating its climate effect. Here, we have developed a new method to retrieve the effective density of internally mixed BC in the atmosphere combining field observations conducted during 15 November -14 December 2016 in urban Beijing with the Köhler theory. The uncertainty of the retrieval method was evaluated within ±30 %, which is primarily caused by assumptions of the hygroscopic parameter of organics and the fraction of primary organic aerosols in non-hygroscopic or hygroscopic mode. Using the method, we obtain that the ambient internally mixed BC, accounting for 80±20 % of total BC aerosol particles, is retrieved with a campaign mean density of 1.1±0.6 g cm^{-3} during the observed periods. The retrieved result is comparable with that reported in the Literature. By applying a lower (0.14 g cm^{-3}) and upper (2.1 g cm^{-3}) limit of the retrieved BC density in cloud condensation nuclei (CCN) number concentrations (N_{CCN}) estimation, we derived that neglect of such variations in BC density would lead to an uncertainty of -28 %~11 % in predicting N_{CCN} at supersaturations of 0.23 % and 0.40 %. We also find that the N_{CCN} is more sensitive to the variations of BC density when it is <1.0 g cm^{-3}. This illustrates a necessity of accounting for the effect of BC density on CCN activity closer to source regions where the BC particles are mostly freshly emitted. The CCN closure achieves when introducing the retrieved real-time BC density and mixing state. This study provides a unique way of utilizing field measurements to infer ambient BC density and

46 highlights the importance of applying variable BC density values in models when

47 predicting CCN and assessing its relevant climate effect.

1 Introduction

49 Black carbon (BC) aerosols, as the major absorber of solar radiation, play a vital

50 role in energy budget and climate of the earth-atmosphere system by affecting the

51 radiative forcing and cloud properties (Flanner et al., 2007; Ramanathan and

52 Carmichael, 2008). The light-absorbing capability induced by BC is related to its

53 density and morphology (Zhang et al., 2008; Rissler et al., 2014), which can be

54 modified after mixing with other atmospheric aerosol particles (Khalizov et al., 2009;

55 Xue et al., 2009). Changes in its physicochemical properties would also regulate its

56 ability to serve as cloud condensation nuclei (CCN) and further indirectly affect the

57 radiative balance by affecting the clouds process (Yuan et al., 2008; Wang et al., 2011).

58 Owing to the complex evolution of the mixing state, density and morphology of BC,

59 the contribution of BC particles to CCN budgets is still not well understood.

60 BC particles, with diesel vehicles, industrial and residential coal combustion as

61 major sources, are ubiquitous in urban environments (Bond et al., 2013; Dameto et al.,

62 2017; Li et al., 2017; Liu et al., 2019a). The mixing state of BC describes the

63 distribution of the bare BC and coating masteries among the aerosol population.

64 Typically, freshly generated BC exists in the form of chain aggregates and initially

65 uncoated, which is known as externally mixed BC (Ex-BC). When the BC particles

66 were emitted, they generally mix with other materials by condensation, coagulation,

67 and other processes (Riemer et al., 2004; Zhang et al., 2008; Liu et al., 2013; Zhang et

68 al., 2020a), forming the internally mixed BC (In-BC) particles consisting of BC core

69 and other chemical components (Cheng et al., 2006; Zhang et al., 2016). The BC

70 structure would be more compact with regular shapes (Pagels et al., 2009; Zhang et al.,

71 2008; Wang et al., 2017), and the effective density of internally mixed BC are changed

72 accordingly with the reconstruction (Liu et al., 2019b). The density and morphology of

73 BC particles are closely related to its sources, mobility size, coating thickness, coating

74 material and its chemical composition (Zhang et al., 2008; Pagels et al., 2009; Peng et

75 al., 2016; Zhang et al., 2022). A wide range of BC density has been reported in previous

76 studies (Lide 1992; McMurry et al., 2002; Park et al., 2004; Kiselev et al., 2010). Recent

77 field measurements have indicated that the average BC density is ~1.2 g cm^{-3} in the

78 ambient atmosphere (Zhang et al., 2016). Field measurements have also indicated that

79 a considerable fraction of externally mixed/uncoated BC exists (Clarke et al., 2004;

80 Cheng et al., 2012), although a higher proportion of internally mixed/aged BC particles

81 in the ambient atmosphere were observed (Schwarz et al., 2008; Massoli et al., 2015;

82 Chen et al., 2020). In climate models, the BC was generally assumed completely

83 internally mixed and treated to have a void-free spherical structure and a density value

84 of 1.8 g cm^{-3} (Bond et al., 2013). This may lead to bias in estimating the climate effect

85 driven by BC.

86   Previous study based on a case study show that when the aging degree of ambient

87 particles is low, the BC density (~1.8 g cm^{-3}) under the spherical assumption will lead

88 to the overestimation of particle hygroscopicity by 40-50 % and the overestimation can

89   be explained almost 100 % using the effective density of fresh BC (~0.45 g cm^{-3}) (Fan

90   et al. 2020). This indicates the importance of using reasonable BC density values in the

91   calculation of particle hygroscopicity. In addition, when estimating the CCN number

92   concentration, a significant bias of –35 % ~ +20 % was found due to the assumption of

93   particle mixing state (Ren et al., 2018). However, these studies have not yet accounted

94   for such impact of BC density and mixing state on CCN prediction due to lack of real

95   time measurement data.

96   The mixing state and the density of BC particles are usually directly measured by

97   several techniques, such as an integrated system of a volatility tandem differential

98   mobility analyzer and a single particle soot photometer (VTDMA-SP2) (Zhang et al.,

99   2016), or a differential mobility analyzer with a SP2 (DMA-SP2) (Olfert et al., 2007;

100   Rissler et al., 2014; Wu et al., 2019), and a differential mobility analyzer–centrifugal

101   particle analyzer–single-particle soot photometer (DMA–CPMA–SP2) system (Liu et

102   al., 2019b; Yu et al., 2020), etc. However, such techniques or measurements are not

103   available in many previously conducted filed campaigns. In this study, we develop a

104   novel method for retrieving the mixing state and effective density of ambient BC

105   particles by combining field measured hygroscopic growth factor and aerosol chemical

106   composition and Köhler theory (Petters and Kreidenweis, 2007). The uncertainty of the

107   new retrieval method was evaluated. The retrieved results were also compared and

108   validated with existing observations. In addition, the effect of BC density and mixing

109   state on prediction of CCN number concentrations is further evaluated through a

110   sensitivity and closure test by accounting for the retrieved real-time variations of BC

111   density and mixing state.

2 Field measurements and methodology

2.1 Field measurements

114   Measurements in this study were conducted from 15 November to 14 December

115   2016 at a typical urban site of Beijing (39.97°N, 116.37°E, 49 m above sea level). The

116   site locates at the Institute of Atmospheric Physics, Chinese Academy of Sciences,

117   which is mainly influenced by the surrounding cooking, road traffic and residential coal

118   burning emissions during the home heating periods (Sun et al., 2016). The detailed

119   information about the sampling site was presented in previous studies (Sun et al., 2015;

120   Zhang et al., 2019). The number concentration of condensation nuclei (CN) at each size

121   was measured by a scanning mobility particle sizer, which is equipped with a

122   differential mobility analyzer (DMA; model 3081, TSI) and a condensation particle

123   counter (CPC; model 3772, TSI). Subsequently, the mono-dispersed particles were

124   introduced into a Droplet Measurement Technologies CCN counter (CCNc, DMT;

125   Lance et al., 2006) to measure CCN number concentration. A hygroscopic tandem

126   differential mobility analyzer (HTDMA) system was used to measure the hygroscopic

127   growth factor (Gf) (Tan er al., 2013). Here, four diameters of 40, 80, 110, 150, and 200

128   nm are selected in the campaign. Gf is defined as the ratio of the mobility diameter at

129   the given RH to the dry diameter (Petters and Kreidenweis, 2007). The nonrefractory

130   submicron aerosol chemical composition was measured by an Aerodyne high-

131   resolution time-of-flight aerosol mass spectrometer (HR-AMS; Xu et al., 2019),

132 including sulfate, nitrate, ammonium, chloride, and organics. Two factors, including a

133 non-hygroscopic primary organic aerosol (POA) and hygroscopic secondary organic

134 aerosol (SOA) were classified by positive matrix factorization (PMF) with PMF

135 algorithm (v4.2) method (Paatero and Tapper, 1994) and followed the procedures

136 reported in Ulbrich et al. (2009). The refractory black carbon mass loading was

137 measured by an aethalometer (model AE33, Magee Scientific Corporation). Both the

138 nonrefractory materials and BC mass concentration were measured with diameters <

139 1.0 μm. The detailed description of the instrument operation and data process have been

140 described in details elsewhere (Ren et al., 2018; Xu et al., 2019; Zhang et al., 2019; Fan

141 et al., 2020).

142 **2.2 Retrieving the mixing state and density of BC**

143 2.2.1 Retrieving the mixing state of BC

144 The Gf probability distribution function (Gf-PDF) for a specified diameter can be

145 retrieved firstly based on the TDMAinv algorithm (Gysel et al., 2009). The κ-PDF can

146 be further calculated based on the Gf-PDF (Fan et al., 2020). Size-resolved κ is derived

147 using κ-Köhler theory based on hygroscopic growth factor (Gf) (Petters and

148 Kreidenweis, 2007),

149
$$\kappa_{gf} = (\text{Gf}^3 - 1) \cdot \left[\frac{1}{\text{RH}} \exp\left(\frac{4\sigma_{s/a} M_w}{RT\rho_w D_d \text{Gf}} \right) - 1 \right] \tag{1}$$

150 where Gf is hygroscopic growth factor, RH is the relative humidity in the HTDMA

151 (90 %), D_d is the dry diameter, $\sigma_{s/a}$ is assumed to be the surface tension of pure water,

152   R is the universal gas constant, T is the temperature, M_w and ρ_w is the molecular mass,

153   and the density of water, respectively.

154   The κ-PDF patterns of particles in different sizes always present two modes: nearly

155   hydrophobic (NH) mode with $\kappa_{gf} \leqslant 0.1$ and more hygroscopic (MH) mode with $\kappa_{gf} >$

156   0.1 (Fig. S1). Firstly, based on the κ-PDF patterns, the number fraction (NF) of the total

157   nearly hydrophobic group with the boundary of [0, 0.1] was calculated according to the

158   following equation:

$$NF = \int_0^{0.1} c(\kappa, D_p) \, d\kappa \tag{2}$$

160   here, the κ-PDF, represented by $c(\kappa, D_p)$, was normalized as $\int c(\kappa, D_p) \, d\kappa = 1$, where

161   κ can be replaced by κ_{gf}, D_p is the selected electrical mobility diameter in the campaign.

162   The nearly hydrophobic mode consists of both externally mixed POA (Ex-POA or

163   bare POA) and externally mixed BC (Ex-BC). Since the number fraction of the nearly-

164   hydrophobic POA would change with the emission and aging processes, in this study,

165   we have applied different values for the number fractions of hydrophobic POA (NH-

166   POA) under clean (91 %), moderately polluted (70 %), and heavily polluted conditions

167   (31 %) by referring the literature (Liu et al., 2021a), as shown in Fig. S2. The number

168   concentration of Ex-BC was then calculated using the total number fraction of NH

169   mode minus the number of NH-POA.

$$N_{POA-containing} = N_{total} \times NF_{POA-containing}$$

$$N_{bare-POA} = N_{POA-containing} \times NF_{bare-POA}$$

$$N_{Ex-BC} = N_{NH} - N_{bare-POA} \tag{3}$$

173   where $N_{POA\text{-}containing}$ and $NF_{POA\text{-}containing}$ are the number concentration and fraction of

174 POA-containing particles, N_{total} is the total number concentration, $N_{bare-POA}$ and NF_{bare-}

175 $_{POA}$ are the number concentration and fraction of bare POA particles, and N_{NH} is the

176 number of nearly hydrophobic group.

177 The number size distribution of the externally mixed BC (n_{Ex-BC} (log D_p)) can be

178 calculated based on the particle number size distribution (PNSD) and the number

179 fraction of the hydrophobic mode of BC (NF_{Ex-BC}) as follows:

180 $$n_{Ex-BC}(\log Dp) = NF_{Ex-BC} \times n\,(\log Dp) \tag{4}$$

181 where n (log D_p) is the function of the aerosol number size distribution, D_p is the

182 mobility diameter.

183 By assuming that the particles are spherical (Rader and McMurry, 1986), the mass

184 size distribution of Ex-BC (M_{Ex-BC}) was obtained as follows:

185 $$M_{Ex-BC}(\log Dp) = \frac{\pi}{6}D_p{}^3 \rho n_{Ex-BC}(\log Dp) \tag{5}$$

186 where D_p is the mobility diameter, ρ is the effective density of Ex-BC, and n_{Ex-BC} (log

187 D_p) is the function of the number size distribution of Ex-BC, respectively. By reviewing

188 and summarizing the existing results, we show that typical values of density for the

189 freshly emitted or externally mixed BC observed in the winter of urban Beijing or North

190 China Plain span over 0.14-0.50 g cm^{-3}, with mean of ~0.40±0.10 g cm^{-3} (Fig. S3), in

191 the size range of 100 to 300 nm, where the mass concentration of externally mixed BC

192 mostly concentrated (Geller et al., 2006; Peng et al., 2016, 2017; Wu et al., 2019; Liu

193 et al., 2020; Zhao et al., 2022). Therefore, an average ρ_{Ex-BC} of 0.4 g cm^{-3} was used for

194 calculating the mass concentration of externally mixed BC in our study. Uncertainty

195 analyses due to the variations of ρ_{Ex-BC} were given in section 2.3.

196   The mass size distribution of Ex-BC was fit using the log-normal distribution as

197   shown in Fig. S4 (Wu et al., 2017; Liu et al., 2019a; Zhao et al., 2022). Thus, the bulk

198   mass concentration of Ex-BC can be calculated from the integration of the mass size

199   distribution:

$$m_{\text{Ex-BC}} = \int_{D_{start}}^{D_{end}} M_{\text{Ex-BC}}(\log D_p) \, d \log(D_p) \tag{6}$$

$$m_{\text{In-BC}} = m_{\text{BC}} - m_{\text{Ex-BC}} \tag{7}$$

202   where D_{start} and D_{end} are the lower and upper size limit, $M_{\text{Ex-BC}}$ ($\log D_p$) is the function

203   of the Ex-BC mass size distribution. We then obtained the bulk mass concentration of

204   internally mixed BC ($m_{\text{In-BC}}$) by subtracting $m_{\text{Ex-BC}}$ from the bulk BC mass

205   concentration measured by AE33 in equation 7. It should be noted that the mass

206   concentration of BC obtained from AE33 based on aerosol light absorption may lead

207   some uncertainty, as has been further addressed in Section 2.3.

208   2.2.2 Retrieving the density of BC

209   For retrieval of the density of BC, the principal idea is to use the measured κ_{gf} to

210   calculate the density of BC based on the Zdanovskii–Stokes–Robinson (ZSR) mixing

211   rule (Stokes and Robinson, 1966; Zdanovskii, 1948) with the chemical composition

212   measured by AMS (Petters & Kreidenweis, 2007). In the retrieval, several aspects are

213   concerned. First, since the ZSR rule assumes the aerosol particles are internally mixed,

214   the κ_{gf} value of the more MH mode ($\kappa_{\text{gf-MH}}$) is thus applied for retrieving the density of

215   internally mixed BC. Second, since the size distribution of BC number concentration is

216   usually with peaks between 100 and 200 nm (Liu et al., 2019a; Yu et al., 2020; Zhao et

217   al., 2022), the $\kappa_{\text{gf-MH}}$ value of particles in accumulation mode was averaged and applied

218   for the retrieval. Previous studies showed an independence of $\kappa_{\text{gf-MH}}$ on particle size

219   when the D_p >100 nm during the campaign period (Fan et al., 2020). Therefore, the

220   average of $\kappa_{\text{gf-MH}}$ in accumulation mode is reasonable for the determination of the In-

221   BC density. In addition, because the inversion including measurements from HTDMA

222   and HR-AMS, a total mass closure of the measured aerosol particles was conducted

223   between the two techniques by comparing the mass concentration of PM_1 and the results

224   are well consistent (Fig. S6). The density of internally mixed BC (In-BC), $\rho_{\text{In-BC}}$ is then

225   derived from the following equations:

226   $\quad \kappa_{gf-MH} = \kappa_{chem} = \sum_i \varepsilon_i \kappa_i = \frac{v_{inorg}}{v_{total}} \kappa_{inorg} + \frac{v_{SOA}}{v_{total}} \kappa_{SOA} + \frac{v_{In-POA}}{v_{total}} \kappa_{POA} + \frac{v_{In-BC}}{v_{total}} \kappa_{BC}$ (8)

227   where $\kappa_{\text{gf-MH}}$ is the hygroscopic parameter of the more hygroscopic (MH) mode, κ_{chem}

228   is the hygroscopic parameter of aerosol particles in the mixed composition and can be

229   calculated based on chemical volume fractions using a simple rule (Stokes and

230   Robinson, 1966; Petters & Kreidenweis, 2007), κ_i is the hygroscopic parameter of each

231   pure composition and ε_i is the volume faction of the individual components in the

232   internally mixed particle. v_{inorg}, v_{SOA} and $v_{\text{In-POA}}$ are the volume of the inorganic, SOA

233   and internally mixed POA species, and can be calculated as follows: $v_{inorg} = \frac{m_{inorg}}{\rho_{inorg}}$,

234   $v_{SOA} = \frac{m_{SOA}}{\rho_{SOA}}$, and $v_{In-POA} = \frac{m_{In-POA}}{\rho_{POA}}$. v_{total} is the total volume of all the species and can be

235   written as $v_{total} = \frac{m_{inorg}}{\rho_{inorg}} + \frac{m_{SOA}}{\rho_{SOA}} + \frac{m_{In-POA}}{\rho_{POA}} + \frac{m_{In-BC}}{\rho_{In-BC}}$. In equation (8), κ_{BC} and κ_{POA} are

236   assumed to be 0. So, the total volume v_{total} can be further written as $v_{total} =$

237   $\frac{v_{inorg}\kappa_{inorg} + v_{SOA}\kappa_{SOA}}{\kappa_{gf-MH}}$. The volume of internally mixed $v_{\text{In-BC}}$ can be calculated as follows,

238   $$v_{In-BC} = \frac{v_{inorg}\kappa_{inorg} + v_{SOA}\kappa_{SOA}}{\kappa_{gf-MH}} - v_{inorg} - v_{SOA} - v_{In-POA}$$

$$239 \qquad = \frac{\frac{m_{inorg}}{\rho_{inorg}}\kappa_{inorg} + \frac{m_{SOA}}{\rho_{SOA}}\kappa_{SOA}}{\kappa_{gf-MH}} - \frac{m_{inorg}}{\rho_{inorg}} - \frac{m_{SOA}}{\rho_{SOA}} - \frac{m_{In-POA}}{\rho_{POA}} \qquad (9)$$

240 Then, the ρ_{In-BC} can be calculated based on its mass concentration and volume as follows:

$$241 \qquad \rho_{In-BC} = \frac{m_{In-BC}}{(\frac{\frac{m_{inorg}}{\rho_{inorg}}\kappa_{inorg} + \frac{m_{SOA}}{\rho_{SOA}}\kappa_{SOA}}{\kappa_{gf-MH}} - \frac{m_{inorg}}{\rho_{inorg}} - \frac{m_{SOA}}{\rho_{SOA}} - \frac{m_{In-POA}}{\rho_{POA}})} \qquad (10)$$

242 where, m_{In-BC} is the mass concentration of internally mixed BC, m_{inorg} and m_{SOA} are the

243 mass concentrations of the inorganic species and SOA, which are measured by the AMS.

244 m_{In-POA} is the mass concentrations of internally mixed POA and can be calculated

245 through subtracting the mass fraction of NH-POA from the total mass concentrations

246 of POA. ρ_{inorg}, ρ_{SOA} and ρ_{POA} are the density of the inorganic species, SOA and POA.

247 Since the AMS measures the concentrations of the organic and inorganic ions, including

248 SO_4^{2-}, NO_3^-, NH_4^+, Cl^-. Here inorganic species were derived by applying a simplified

249 ion pairing scheme (Gysel et al., 2007) to convert mass concentrations of ions to the

250 inorganic salts as follows:

$$252 \qquad n_{\mathrm{NH_4NO_3}} = n_{\mathrm{NO_3^-}}$$

$$253 \qquad n_{\mathrm{NH_4HSO_4}} = \min(2n_{\mathrm{SO_4^{2-}}} - n_{\mathrm{NH_4^+}} + n_{\mathrm{NO_3^-}}, n_{\mathrm{NH_4^+}} - n_{\mathrm{NO_3^-}})$$

$$254 \qquad n_{\mathrm{(NH_4)_2SO_4}} = \max(n_{\mathrm{NH_4^+}} - n_{\mathrm{NO_3^-}} - n_{\mathrm{SO_4^{2-}}}, 0)$$

$$251 \qquad n_{\mathrm{H_2SO_4}} = \max(0, n_{\mathrm{SO_4^{2-}}} - n_{\mathrm{NH_4^+}} + n_{\mathrm{NO_3^-}}) \qquad (11)$$

255 where n represents the number of moles, and the mass concentrations were obtained by

256 the number of moles times the molar mass of each inorganic salts. Because the value of

257 the $n_{\mathrm{H_2SO_4}}$ was zero in this campaign. Three inorganic salts including NH_4HSO_4,

258 $(NH_4)_2SO_4$, and NH_4NO_3 were applied in our study. The densities for inorganic salts

259 were taken from previous studies (Gysel et al., 2007; Wu et al., 2016). Here the densities

260 for three inorganics are 1.78, 1.77 and 1.72 g cm^{-3}, respectively. By summarizing the

261 previous studies (Gysel et al., 2007; Dinar et al., 2006), 1.4 g cm^{-3} was selected as the

262 density of SOA (ρ_{SOA}). The density of POA (ρ_{POA}) is assumed to be 1.0 g cm^{-3} for urban

263 environments, which is similar to the that of the lubricating oil (Wu et al., 2016). Since

264 the cooking organic aerosols represent a high contribution to POA in urban

265 environments, we choose the mean density of the rapeseed oil and oleic acid (~0.85 g

266 cm^{-3}) (Reyes-Villegas et al., 2018) to evaluated the result as shown in section 2.3. The

267 values of κ for inorganic components are 0.56 for NH$_4$HSO$_4$, 0.48 for (NH$_4$)$_2$SO$_4$ and

268 0.58 for NH$_4$NO$_3$, along with the best-fit values for the three inorganic salts (Petters &

269 Kreidenweis, 2007 and Gunthe et al., 2009). The κ_{SOA} is assumed to be 0.15 according

270 to the field studies in urban areas (Chang et al., 2010; Kawana et al., 2016).

271   Note that the method fails to retrieve the BC density when organic accounts for a

272 large fraction (>60 %). This is because that a higher fraction of OA usually corresponds

273 to lower total volume of all the species (Fig. S7), yielding negative values for v_{In-BC}

274 introduced in equation 9. As a result, 61 % of the data observed during the campaign

275 were valid for calculating the BC density.

276   Similarly, the bulk density of BC ($\rho_{bulk-BC}$) is calculated with the same method as

277 that for calculating the $\rho_{In-BC.}$ When calculating the $\rho_{bulk-BC}$, the bulk κ_{gf} value measured

278 by HTDMA is applied assuming that all the aerosol particles are internally mixed.

279 **2.3 Uncertainties and limitations**

280   For the retrieval, the assumptions on the values of κ_{SOA}, ρ_{POA}, ρ_{SOA} and ρ_{Ex-BC} as

281 well as the fraction of primary organic aerosols in non-hygroscopic or hygroscopic

282   mode would add uncertainty in the inferred values of ambient internally mixed BC

283   density. For example, the freshly emitted POA particles might consistently be coated

284   with the secondary particles during the aging process, resulting in changes of the $NF_{NH\text{-}}$

285    $_{POA}$. However, a real-time variation of the $NF_{NH\text{-}POA}$ is not yet available due to the lack

286   of such measurements data. Applying only the rough fractions of hydrophobic POA for
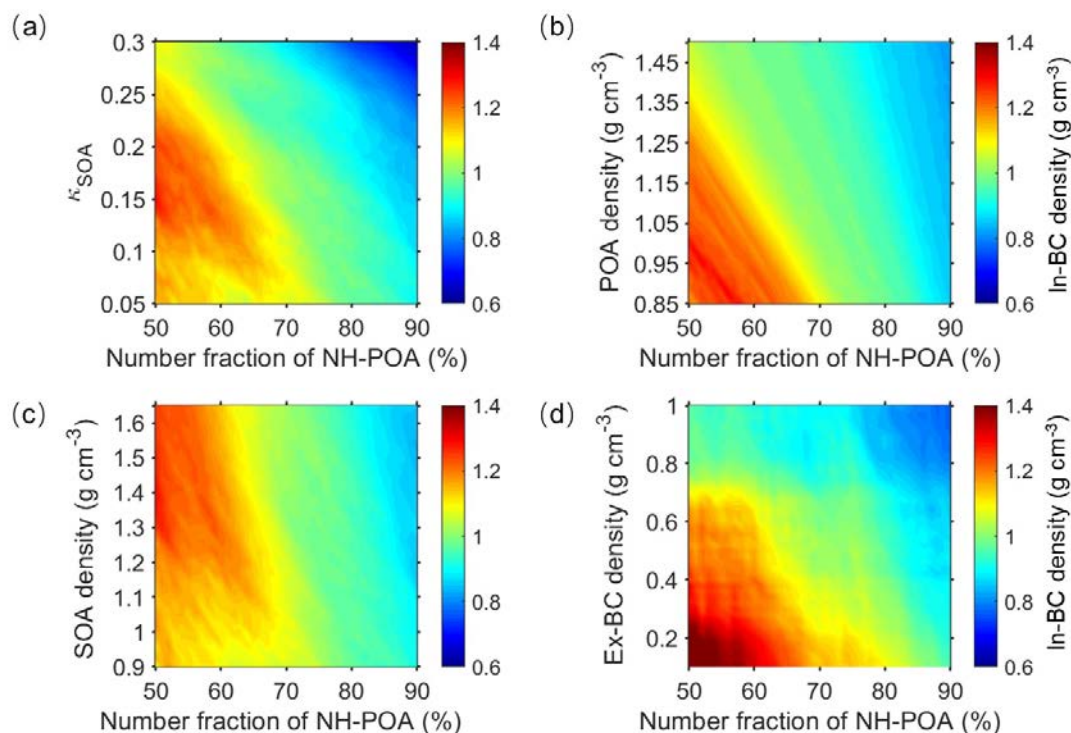
287

288   **Figure 1.** Sensitivities of In-BC density to the variations in the number fraction of

289   nearly hydrophobic (NH) POA and hygroscopic parameter of OA (k_{SOA}) (a), POA

290   density (b), SOA density (c) and the externally mixed BC density (d).

291   three different atmospheric conditions could still cause uncertainties. Also, the densities

292   of POA and SOA may differ due to their precursors, emission sources and the formation

293   mechanisms in ambient atmosphere (Alfarra et al., 2006; Reyes-Villegas et al., 2018).

294   And the density of Ex-BC is generally characterized by the morphology and size (Wu

295   et al., 2019). In addition, the value of k_{SOA} spans largely due to the variability in the

296   emissions of gas precursors and formation processes under different atmospheric

297   conditions (Zhang et al., 2015; Liu et al., 2021b). Therefore, we examined the

298   sensitivities of In-BC density to the variations of these factors, as exhibited in Fig. 1

299   and Fig.2.
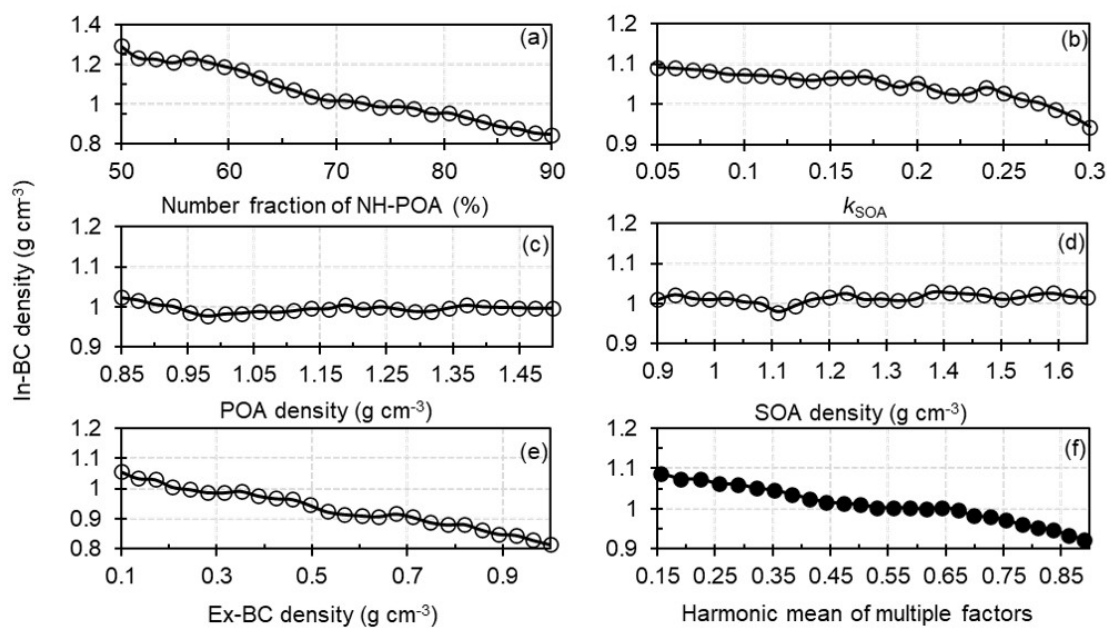
300

301   **Figure 2.** Sensitivity of the In-BC density to variations in the number fraction of nearly

302   hydrophobic (NH) POA (a), the hygroscopic parameter of SOA (b), the POA density

303   (c), the SOA density (d), the externally mixed BC density (e) and the harmonic mean

304   of multiple factors (f).

305   The figures show that the In-BC density gradually decreases with the increment of

306   the $NF_{NH\text{-}POA}$, implying the high fraction of bare POA particles correspond to the early

307   aging stage of aerosol particles. With increase of κ_{SOA}, the In-BC density is generally

308   reduced, but with small fluctuations (Fig.1a, Fig. 2b). This suggests a complex impact

309   of assumptions of κ_{SOA} on the retrieved BC density. In addition, the In-BC density

310   decreases slightly as $\rho_{Ex\text{-}BC}$ increases (Fig. 2e), suggesting applying a larger $\rho_{Ex\text{-}BC}$

311   would derive smaller values for In-BC density. The In-BC density is insensitive to the

312   changes of the density of POA and SOA, showing an almost negligible effect on the

313   retrieved results (Fig. 2c and d).

314   The uncertainty analysis shows that, by comparing the results based on the mean

315   fractions of the $NF_{\text{NH-POA}}$ with a typical atmospheric observed range of 50-90 % for the

316    $NF_{\text{NH-POA}}$ (Liu et al., 2021a), we show that the assumption on $NF_{\text{NH-POA}}$ can lead to

317   relative deviations (uncertainty) of -17 %~+27 % for the retrieved BC density (Fig.3a).
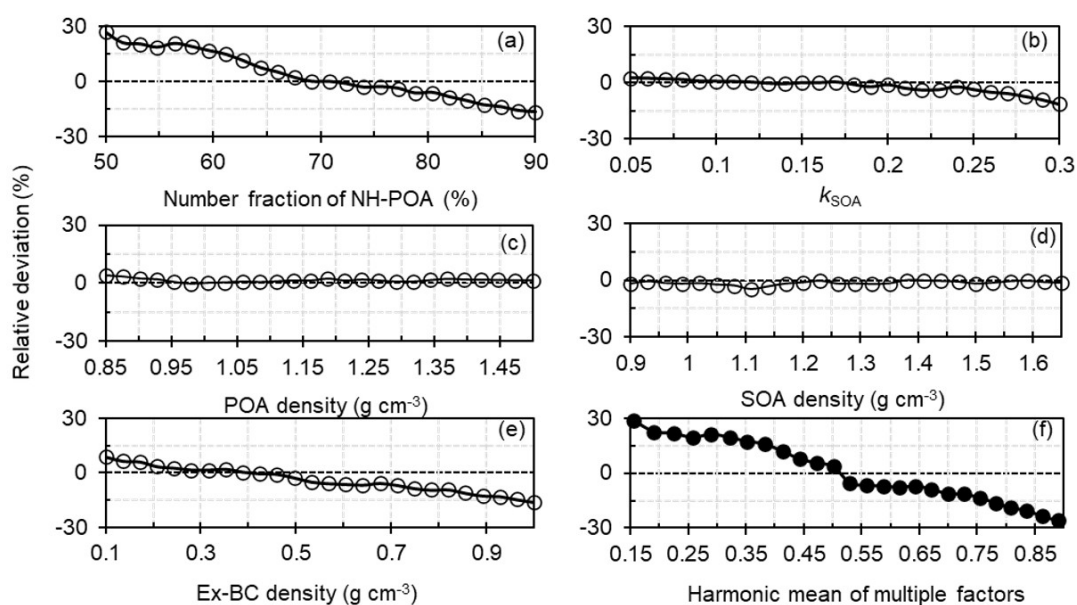
318

319   **Figure 3.** Relative deviations of the number fraction of nearly hydrophobic (NH) POA

320   to the In-BC density (a), the hygroscopic parameter of OA to the In-BC density (b), the

321   POA density to the In-BC density (c), the SOA density to the In-BC density (d), the

322   externally mixed BC density to In-BC density (e) and the combined deviations based

323   on multiple factors mentioned above (f).

324   In addition, unlike inorganics (eg., NH_4HSO_4, $(NH_4)_2SO_4$ and NH_4NO_3), which

325   the hygroscopicity has been already well-understood (Petters and Kreidenweis, 2007),

326   the hygroscopicity of organic species varies largely due to the complexity in organic

327   aerosol constituents. Therefore, the assumption of the values of κ_{SOA} will add the

328   uncertainty in the calculation of BC density. Previous studies have suggested that the

329   organics has a wide range of κ values ranging from 0.05 to 0.3 (Jimenez et al., 2009;

330   Mei et al., 2013). Thus, the sensitivity test has also been done to examine the effect due

331   to changes in κ_{SOA} on calculating the density of BC (Fig. 1a). The result shows that the

332   assumption of κ_{SOA} value can cause an average relative deviation of -10 %~+3 % in

333   calculating the density of In-BC (Fig. 3b).

334   However, the sensitivity test shows that the impact of both the ρ_{POA} and ρ_{SOA}

335   variations on the BC density estimation is very small or even negligible (Fig. 1b, c). By

336   varying the ρ_{POA} from 0.85 to 1.5 g cm^{-3} and the ρ_{SOA} from 0.9 to 1.65 g cm^{-3} according

337   to the literatures (Noureddini et al., 1992; Alfarra et al., 2006; Reyes-Villegas et al.,

338   2018; Cai et al., 2020; Kostenidou et al., 2007), the retrieval uncertainties in the BC

339   density are both within ±5 % (Fig. 3c, d). For ρ_{Ex-BC}, it exhibits that the evolution of the

340   ρ_{Ex-BC} could lead to an average deviation of -16 %~+9 % in calculating In-BC density

341   (Fig. 3e) when increasing the values of ρ_{Ex-BC} from 0.1 to 1.0 g cm^{-3}, which represents

342   a typical range in ambient atmosphere (Wu et al., 2019; Liu et al., 2020). A combined

343   uncertainty (δ) caused by the multiple factors (δ_i), which is calculated by equation 12,

344   is -26 %~+29 % as shown in Fig. 3f.

345    $$\delta = \sqrt{\sum_{i=1}^{n} \delta_i^2} \qquad (12)$$

346   In addition, it should be noted that the mass concentration of BC obtained from

347   AE33 based on aerosol light absorption may lead some uncertainty. However, the

comparison of the simultaneously measured data by SP2 with that by AE33 during the campaign shows that the temporal variations of BC mass concentrations measured by the two techniques are well consistent (Fig S5). Note that the BC mass measured by SP2 is occasionally low probably because of the low detection efficiency in small size (McMeeking et al., 2010; Schwarz et al., 2006). In addition, the SP2 is unable to quantify the BC mass beyond a certain limit because of the saturation of electronic devices recording signals (Pileci et al., 2021). We show that, compared the results that retrieved if applying the BC mass measured by SP2, the BC density retrieved based on AE33 can be 18% higher. Given that the measurement bias from SP2, this overestimation indicates an upper limit of the uncertainty.

3 Results and Discussion

3.1 Retrieved mixing state and density of BC: comparison and validation

Figure 4a shows retrieved time series of the mixing state of ambient BC during the campaign. Large temporal variations of the mass fraction of internally and externally mixed BC are presented during the observed period at the sites. The temporal changes should be related to the atmospheric aging process or diurnal variations of emissions (Liu et al., 2019a; Fan et al., 2020). Statistically, the average mass fraction of externally and internally mixed BC is 20±18 % and 80±20 % respectively, showing that most of the BC particles were aged and internally mixed with other components. Previous studies at urban sites have shown that the co-existence of the externally mixed BC in the ambient atmosphere (Schwarz et al., 2008; Cheng et al., 2012; Chen et al., 2020)

due to continuous combustion processes (e.g., vehicle exhaust and residential sector)

(Wang et al., 2017; Liu et al., 2019a). Our results are basically comparable with those
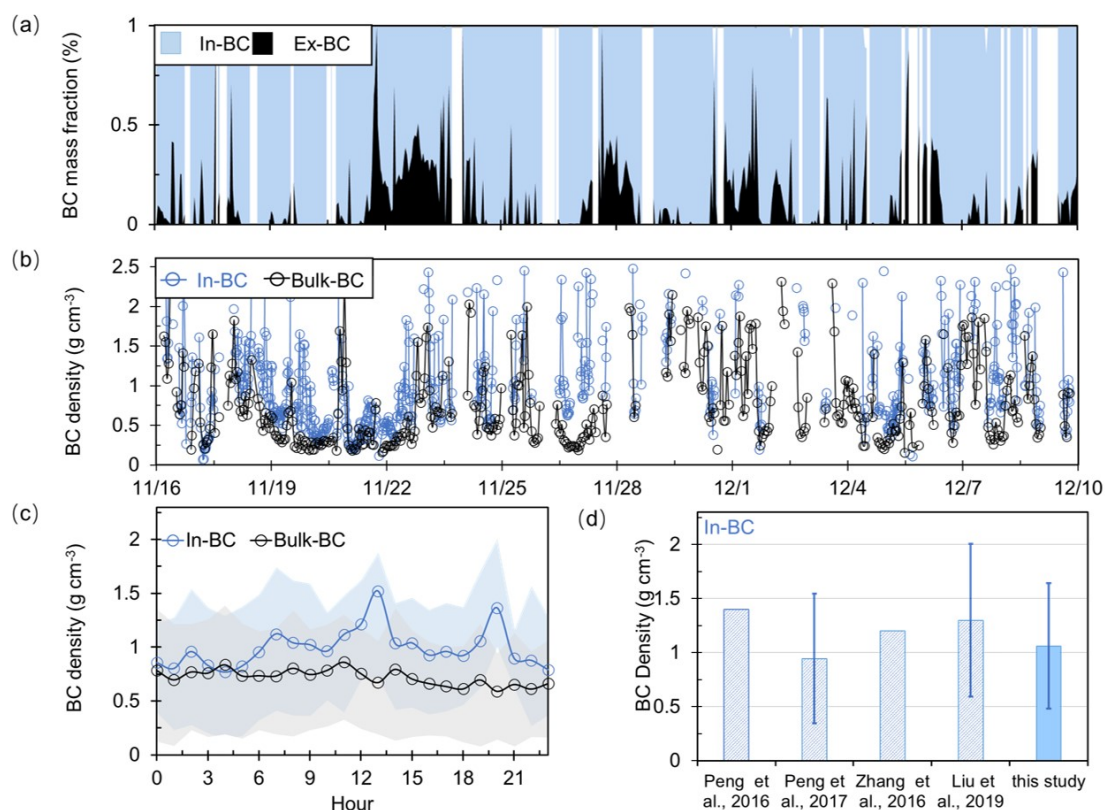
Figure 4. (a) Time series of the mass fraction of the retrieved internal- and external-

mixed BC; (b) Time series of the retrieved density of the bulk and internal- mixed BC

(In-BC); (c) Diurnal variation of the retrieved density of bulk and In-BC; (d)

Comparison of the results of the derived In-BC density in this study with that reported

in literatures.

previously reported results, which are directly measured or indirectly retrieved. For

example, Chen et al., 2020 found that the mass fraction of internally mixed BC particles

was nearly ~80−90 % in summer of Beijing based on VTDMA measurements. Liu et al.

(2020), using a tandem system with an aerodynamic aerosol classifier and SP2, reported

that the mass fraction of internally BC-containing particles would increase with

382   increasing size and reach ~70 % in Beijing. Overall, the mass fraction obtained in our

383   study is comparable with those reported in urban Beijing. Previous studies also

384   displayed that the significant diversity of the BC mixing state among emission

385   conditions and coating process (Shiraiwa et al., 2008; Pan et al., 2017; Zhang et al.,

386   2020b). Accordingly, the densities of the bulk and internally mixed BC present apparent

387   fluctuations as shown in Fig. 4b, which is significantly affected by the variations of BC

388   emission sources and its rapid aging process. The density of the In-BC during daytime

389   was generally higher than that at night (Fig. 4c). The elevated BC density during

390   daytime is likely due to that the strong photochemical processes promote the aging of

391   BC particles, which resulted in a conversion from uncompacted structure to compact

392   and regular spherical shapes of BC (Qiao et al., 2018; Liu et al., 2019b; Zhou et al.,

393   2022). The lift in BC density around 20:00 LT might indicate that the BC particles

394   would be rapidly coated with the secondary inorganic aerosol (SIA) particles and

395   continuously aged in the polluted period due to the heterogeneous reactions of SIA in

396   urban regions (Zhang et al., 2016; Peng et al., 2017). Actually, following the haze

397   evolution, the fraction of nearly hydrophobic group reduced rapidly (Fig. S8).

398   Consequently, the average density of In-BC increased obviously from the clean

399   conditions to the polluted periods (Fig. S9). A slight decrease was observed in the bulk

400   BC density during traffic hours. This is likely associated with the continues emissions

401   (e.g., vehicle exhaust) that lead to uncoated or uncompacted BC particles in this period.

402   The diurnal cycle in In-BC density is consistent with the coating thickness measured

403   by a tandem CPMA-SP2-DMA-SP2 (Liu et al., 2020), demonstrating that the new

404 method can derive the density of ambient BC particles reasonably. Averagely, the bulk

405 and internally mixed BC densities are with campaign averaged values of 0.7±0.5 and

406 1.1±0.6 g cm^{-3} respectively, which are much less than 1.8 g cm^{-3}, implying that the BC

407 particles is not a void-free spheres in the urban atmosphere. The results of In-BC density

408 are comparable with that observed at the other sites in North China Plain (NCP) as

409 shown in Fig. 4d, illustrating that the BC effective density retrieved by this method is

410 within the range of field measurements.
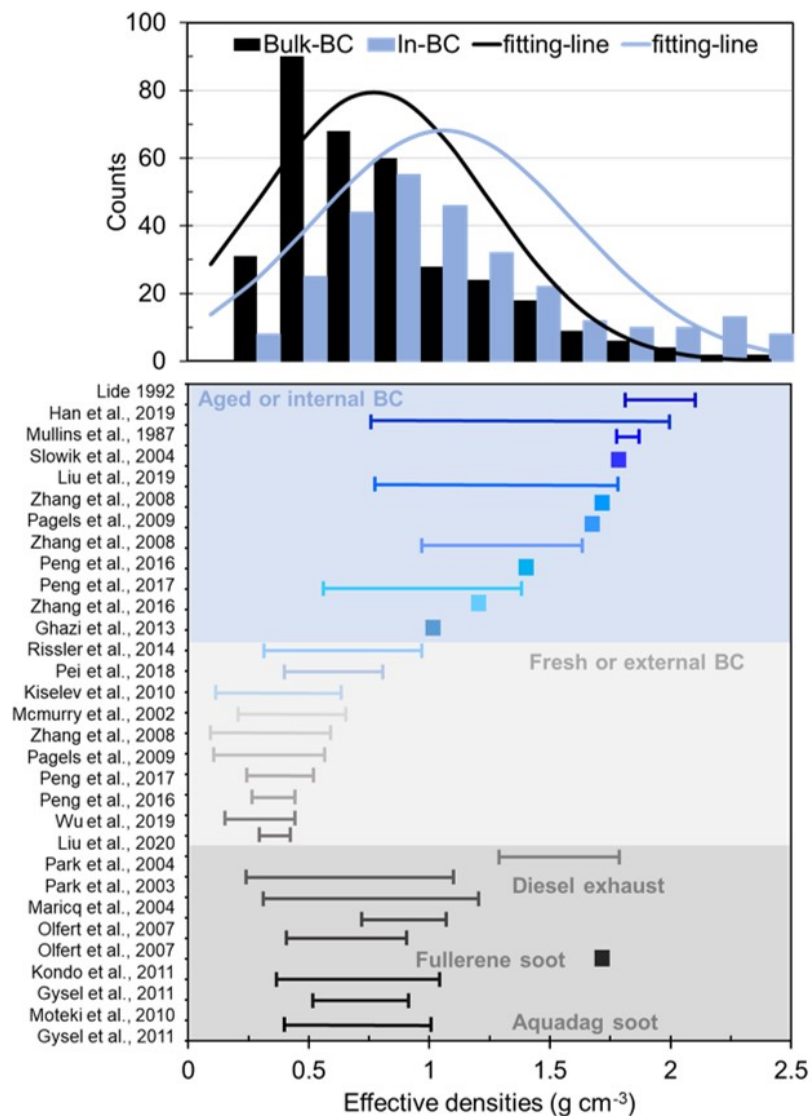
411

412 **Figure 5.** The probability distribution function (PDF) of the retrieved density of bulk

413 and In-BC and the measured density distribution spectrum of BC from different sources

414   reported in literatures.

415   Based on both field measurements (e.g. Lide 1992; Zhang et al., 2016; Wu et al.,

416   2019; Liu et al., 2019b) and laboratory studies (e.g. McMurry et al., 2002; Park et al.,

417   2003, 2004; Olfert et al., 2007; Kiselev et al., 2010; Gysel et al., 2011, 2012), the BC

418   density from diverse combustion sources or representing different aging degree has

419   been obtained and ranges widely from 0.14 to 2.1 g cm^{-3}, as has been summarized and

420   shown in Fig. 5. Mean probability distribution function (PDF) of the density of bulk

421   and In-BC retrieved by this study is also presented in Fig. 5. It shows that the retrieved

422   density of bulk BC exhibits a dominant mode with a peak value of 0.7 g cm^{-3}, which is

423   situated between the typical density range of those externally mixed and internally

424   mixed BC measured previously. For the In-BC, the PDF is with a peak value at 1.1 g

425   cm^{-3}, but ranges widely from ~0.5 to 2.5 g cm^{-3}, which indicates various morphologies,

426   different aging degree and compositions of ambient BC particles due to the complex

427   impact of multiple local sources and aging processes during the observed period in

428   urban Beijing. Overall, the retrieved values for In-BC density fall within the range of

429   typical internal mixed BC reported in the literatures, verifying the reliability of our

430   inversion results.

431   **3.2 Sensitivity of predicted N_{CCN} to changes of BC density**

432   A previous study showed that the use of an inaccurate density value of BC particles

433   would result in large bias in estimating κ of ambient aerosol particles with the ZSR

434   mixing rule (Fan et al., 2020), as would further lead to uncertainties in prediction of

435   N_{CCN} and relevant climate effects. Considering the large variation range of BC density

436   during the campaign, which is closely associated with its morphology or degree of its

437   aging, we further examine the sensitivity of critical supersaturation (S_c), critical

438   diameter (D_{cut}) and predicted N_{CCN} to variations of BC density (Fig. 6). Here, we use

439   the critical diameter and particle number size distribution to calculate N_{CCN}. The method

440   to derive the critical diameter is based on Köhler theory and ZSR rule.
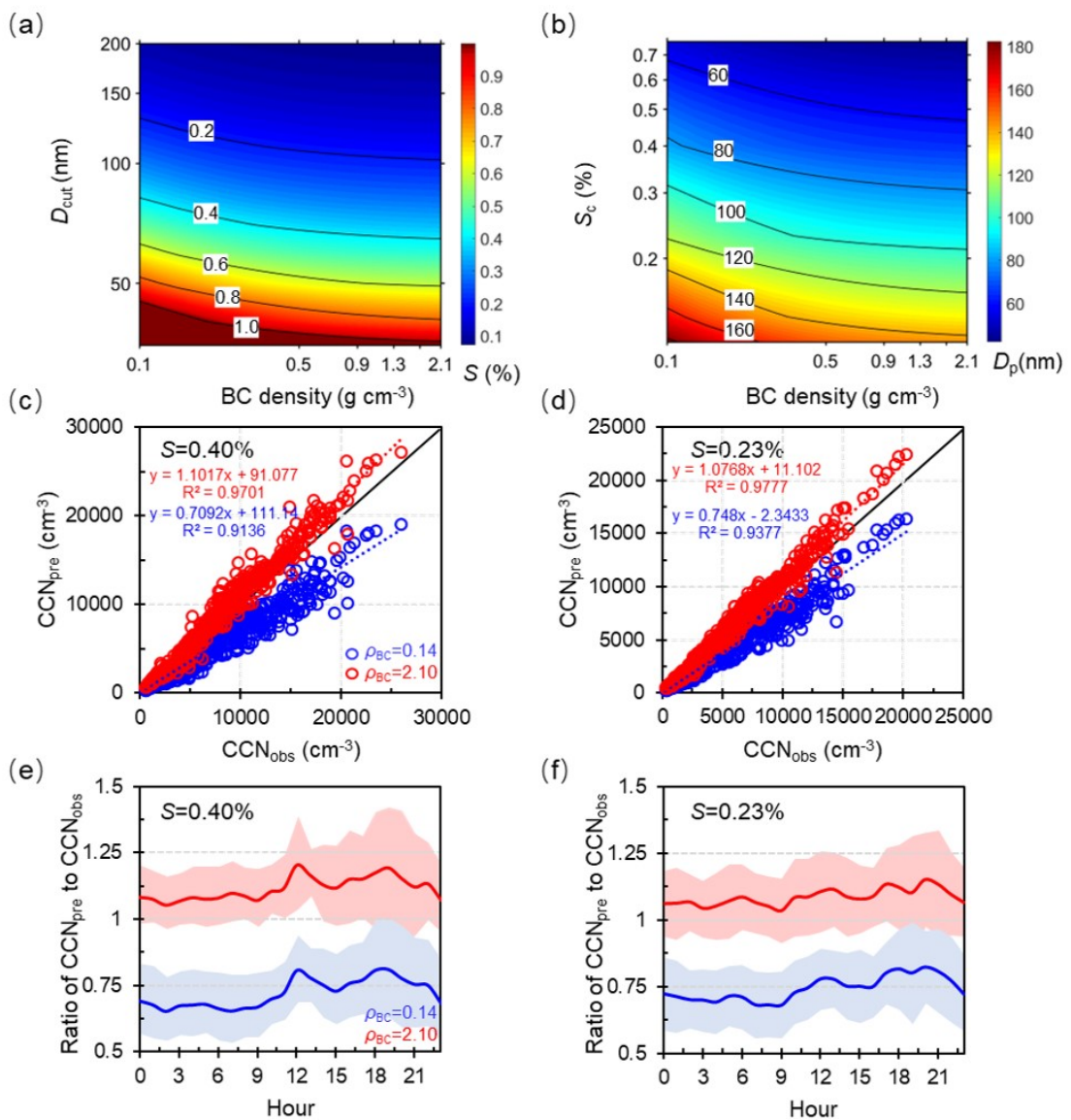
441

442   **Figure 6.** Sensitivity of critical supersaturation (S_c) (a) and diameter (D_{cut}) (b) to the

443   variations in BC density; Predicted N_{CCN} as a function of measured N_{CCN} by varying the

444   density from 0.14 to 2.1 g cm^{-3} at S=0.40 % (c) and S=0.23 % (d), the black solid line

445   is the 1:1 line; Diurnal variations in the ratio of predicted-to-measured N_{CCN} at S=0.40 %

446   (e) and S=0.23 % (f).

447   The results show that, by varying the value of density from 0.14 to 2.1 g cm^{-3} that

448   represents the lower and upper limit of BC density in the atmosphere, the D_{cut} reduces

449   apparently at a given supersaturation (S) (Fig. 6a), or similarly, the S_c decreases rapidly

450   for a given particle size (Fig. 6b). The results show that the changes of the D_{cut} and S_c

451   are more sensitive when the BC density is below 1.0 g cm^{-3}. And the effects on the D_{cut}

452   and S_c both gradually weakened with the increase of BC density. This shows that it is

453   critical to apply more accurate BC density for the aerosol particles with low aging

454   degree in predicting CCN and its climate effect. Accordingly, the ratios of predicted-

455   to-measured N_{CCN} ranged from 0.72 to 1.11 by varying the BC density from 0.14 to 2.1

456   g cm^{-3} at the typical S of 0.23 % and 0.40 % (Fig. 6c, 6d), showing an estimation

457   uncertainty of -28 % ~ 11 % in N_{CCN} prediction.

458   The diurnal variations in the ratio of predicted-to-measured N_{CCN} at S=0.40 % and

459   0.23 % are shown to examine the response of the BC density on N_{CCN} prediction at

460   different time periods (Fig. 6e, 6f). By applying the lower limit of density value of 0.14

461   g cm^{-3}, the prediction is much worse compared to the use of the density of 2.1 g cm^{-3} at

462   nighttime (00:00-06:00 LT), when the latter is much closer to the real density of ambient

463   BC (Fig. 4c). The prediction is improved substantially by applying the value of 0.14 g

464   cm^{-3} during evening rush hours (18:00-20:00 LT), during which the ambient BC

465   particles is disturbed by the traffic emissions (Fig. 4c). And now, the prediction becomes

466 worse by applying the value of 2.1 g cm^{-3}, and an obvious overestimation by up to ~40 %

467 is shown. The results further illustrate that it is critical to account for the real-time

468 mixing state and density of BC particles in N_{CCN} prediction, particularly in those regions

469 with heavy traffic and residential coal emissions.

470   It should be noted that the assumption of the surface tension of water would

471 overestimate the critical diameter and underpredict CCN number concentration. While

472 the surface tension depression might be more obvious for the small size particles (<60

473 nm), as the fraction of organics are higher at small particles size (Meng et al., 2014; Cai

474 et al., 2018). Here, in this study, we calculated the critical diameters at supersaturations

475 of 0.40 % and 0.23 %, typical values in cloud, corresponding to larger sizes (> 70 nm

476 and 90 nm) of aerosols. Therefore, the uncertainties from the application of the surface

477 tension of pure water should be negligible (< 10 %). Here, three schemes were assumed

478 to evaluate the effect of BC density and mixing state on prediction of CCN number

479 concentrations. The detailed calculation methods are presented in the supporting

480 information (SI: Methods) or referenced from Ren et al. (2018).

481 **3.3 Using the real-time variations of BC density and mixing state to predict N_{CCN}**

482   Figure 7 exhibits the comparisons between predicted and measured N_{CCN} at S of

483 0.23 % and 0.40 % by accounting for the retrieved real-time variations of BC density

484 and mixing state. It shows that the N_{CCN} can be well predicted with a slope of 1.01 and

485 1.02 at S of 0.23 % and 0.40 % respectively (Fig. 7a, 7b), only presenting a slight

486 deviation. The slight deviation is primarily due to the fixed value of the density for the

487 externally mixed BC caused by the retrieved method, especially during noontime and

488 evening rush periods (Fig. 7c and 7d).
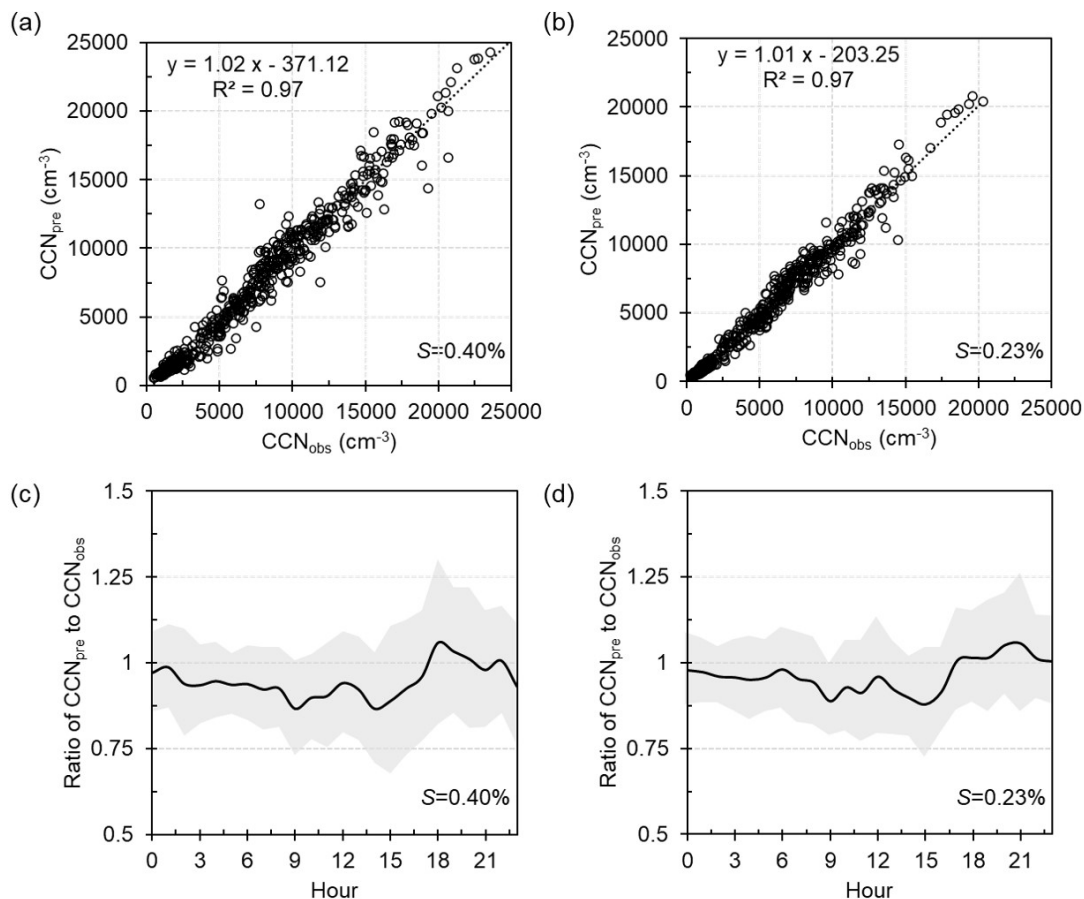
489

490 **Figure 7.** Prediction CCN number concentration using the mixing state and In-BC

491 density derived from HTDMAs at S=0.40 % (a) and S=0.23 % (b). Diurnal variations

492 in the ratio of predicted-to-measured N_{CCN} at S=0.40 % (c) and S=0.23 % (d).

493   The diurnal variations in the ratio of predicted-to-measured N_{CCN} shows the N_{CCN}

494 can be underestimated by up to 15 % at S=0.40 % during those periods. While, a slightly

495 overrated during the evening traffic hours and nighttime may be due to the

496 underestimation of the number fraction of Ex-BC. Overall, the dependence of the CCN

497 prediction on S is due to the size dependence of κ and mixing state (Zhang et al., 2017;

498 Liu et al., 2020; Xu et al., 2021). The better closure at S=0.23 % is because that the bulk

499   κ of particles is closer to that the critical diameter corresponding to S=0.23 %, with D_p

500   of 100-150 nm. Similarly, the effect on CCN prediction induced by the bulk mixing

501   state would be more critical for smaller particles, corresponding to the critical diameter

502   at high S.

503   Overall, when considering the effective density of BC relevant to its mixing state,

504   the CCN closure achieves. Previous studies have shown that the fresh emitted BC

505   particles may convert from fractal-like aggregates to a compact structure and its density

506   would increase with the aging process (Pagels et al., 2009; Rissler et al., 2014; Peng et

507   al., 2016; Liu et al., 2019b; Zhang et al., 2020a, 2022), but the actual density of In-BC

508   may be lower than 1.8 g cm^{-3} in the ambient atmosphere according to this study.

509   Therefore, the currently applied value represents a density of the void-free structure of

510   BC particles may cause an overestimation in CCN prediction.

511   **4 Conclusions**

512   The mixing state and effective density of BC changed through heterogenous

513   chemistry process and thus would cause uncertainty in evaluating its CCN activity. In

514   this study, we develop a new method to retrieve the mixing state and effective density

515   of ambient BC using field measurements and the Köhler theory. The uncertainty of the

516   new retrieval method was evaluated within ±30 %, which is primarily caused by

517   assuming the value of κ_SOA and the fraction of primary organic aerosols in non-

518   hygroscopic mode. The retrieved results show that most of the BC particles were aged

519   and internally mixed with other components, with mean mass fraction of 80±20 %.

520   Averagely, the retrieved densities of the bulk and internally mixed BC are 0.7±0.5 and

521   1.1±0.6 g cm^{-3} respectively, but ranges widely from ~0.1 to 2.5 g cm^{-3}, indicating

522   various morphologies, different aging degree and compositions of ambient BC particles

523   due to the complex impact of multiple local sources and aging processes during the

524   observed period. The retrieved results are basically comparable with the previous

525   observations in North China Plain.

526   Further examination shows the N_{CCN} prediction is with uncertainties of -28 % ~11 %

527   at the typical S of 0.23 % and 0.40 % by varying the BC density from 0.14 to 2.1 g cm^{-3}

528   that represents the lower and upper limit of ambient BC particles. Moreover, the

529   prediction is found more sensitive to the variability of BC density when it is <1.0 g cm^{-3},

530   suggesting a great significance to account for the effect of BC density for the aerosol

531   particles with low aging degree when evaluating the climate effect. The CCN closure

532   achieves when introducing the retrieved real-time BC density relevant to its mixing

533   state. This work provides a unique way of utilizing field observations to infer ambient

534   BC density and highlights the current assumption of a void-free structure of BC

535   particles in models would cause large uncertainties in CCN prediction and in the

536   relevant climate effect evaluation.

537   The method used to derive the ambient BC density has limitations. Since the

538   assumptions on the values of κ_{SOA}, ρ_{POA}, ρ_{SOA} and ρ_{Ex-BC} as well as the fraction of

539   primary organic aerosols in non-hygroscopic or hygroscopic mode would add

540   uncertainty in the inferred values of ambient internally mixed BC density. It is thus

541   necessary to examine observational data to verify this methodology in further studies.

However, the method and results of this study could provide the way for a more comprehensive understanding of the variability in BC density in Beijing. Additionally, it has the potential to reveal the uncertainties of usage of void-free structure of BC density in accessing the climate effects.

Data availability.

All data needed to evaluate the conclusions in the paper are present in the paper and/or the Supplement. All data used in the study are also available from the corresponding author upon request (zhangfang2021@hit.edu.cn).

Author contributions.

FZ and JR conceived the conceptual development of the manuscript. JR directed and performed of the experiments with JL, LC, and FZ. JR conducted the data analysis and wrote the draft of the manuscript. All authors edited and commented on the various sections of the manuscript.

Acknowledgments.

This work was funded by the National Natural Science Foundation of China (NSFC) research project (41975174, 41675141). We thank all participants in the field campaigns for their tireless work and cooperation. We also thank Dr. Yele Sun and his group for providing the data of nonrefractory submicron aerosol chemical composition.

Competing interests.

The contact author has declared that neither they nor their co-authors have any competing interests.

References

Alfarra, M. R., Paulsen, D., Gysel, M., Garforth, A. A., Dommen, J., Prévôt, A. S. H., Worsnop, D. R., Baltensperger, U., and Coe, H.: A mass spectrometric study of secondary organic aerosols formed from the photooxidation of anthropogenic and biogenic precursors in a reaction chamber, Atmos. Chem. Phys., 6, 5279– 5293, https://doi:10.5194/acp-6-5279-2006, 2006.

Bond, T. C., Doherty, S. J., Fahey, D., Forster, P., Berntsen, T., DeAngelo, B., Flanner, M., Ghan, S., Kärcher, B., and Koch, D.: Bounding the role of black carbon in the climate system: A scientific assessment, J. Geophys. Res.-Atmos., 118(11), 5380– 5552, https://doi.org/10.1002/jgrd.50171, 2013

Clarke, A.D., Shinozuka, Y., Kapustin, V.N., Howell, S., Huebert, B., Doherty, S., Anderson, T., Covert, D., Anderson, J., Hua, X., Moore II, K.G., McNaughton, C., Carmichael, G., Weber, R.: Size distributions and mixtures of dust and black carbon aerosol in Asian outflow: physiochemistry and optical properties, J. Geophys. Res.-Atmos., 109, D15S09, https://doi.org/10.1029/2003JD004378, 2004.

Cheng, Y. F., Su, H., Rose, D., Gunthe, S. S., Berghof, M., Wehner, B., Achtert, P., Nowak, A., Takegawa, N., Kondo, Y., Shiraiwa, M., Gong, Y. G., Shao, M., Hu, M., Zhu, T., Zhang, Y. H., Carmichael, G. R., Wiedensohler, A., Andreae, M. O., and Pöschl, U.: Size-resolved measurement of the mixing state of soot in the megacity Beijing, China: diurnal cycle, aging and parameterization, Atmos. Chem. Phys., 12, 4477–4491, https://doi.org/10.5194/acp-12-4477-2012, 2012.

Cheng, Y. F., Eichler, H., Wiedensohler, A., Heintzenberg, J., Zhang, Y. H., Hu, M., Herrmann, H., Zeng, L. M., Liu, S., Gnauk, T., Brüggemann, E., and He, L. Y.: Mixing state of elemental carbon and non-light-absorbing aerosol components derived from in situ particle optical properties at Xinken in Pearl River Delta of China, J. Geophys. Res., 111, D20204, doi:10.1029/2005JD006929, 2006.

Chen, L., F. Zhang, P. Yan, X. Wang, L. Sun, Y. Li, X. Zhang, Y. Sun, and Z. Li.: The large proportion of black carbon (BC)-containing aerosols in the urban atmosphere, Environ. Pollut., 263, 114507, https://doi.org/10.1016/j.envpol.2020.114507, 2020.

Chang, R. Y.-W., Slowik, J. G., Shantz, N. C., Vlasenko, A., Liggio, J., Sjostedt, S. J., Leaitch, W. R., and Abbatt, J. P. D.: The hygroscopicity parameter (k) of ambient organic aerosol at a field site subject to biogenic and anthropogenic influences: relationship to degree of aerosol oxidation, Atmos. Chem. Phys., 10, 5047–5064,

https://doi:10.5194/acp-10-5047-2010, 2010.

Cai, M., Tan, H., Chan, C. K., Qin, Y., Xu, H., Li, F., Schurman, M. I., Liu, L., and Zhao, J.: The size-resolved cloud condensation nuclei (CCN) activity and its prediction based on aerosol hygroscopicity and composition in the Pearl Delta River (PRD) region during wintertime 2014, Atmos. Chem. Phys., 18, 16419–16437, https://doi.org/10.5194/acp-18-16419-2018, 2018.

Cai, J., Chu, B., Yao, L., Yan, C., Heikkinen, L. M., Zheng, F., Li, C., Fan, X., Zhang, S., Yang, D., Wang, Y., Kokkonen, T. V., Chan, T., Zhou, Y., Dada, L., Liu, Y., He, H., Paasonen, P., Kujansuu, J. T., Petäjä, T., Mohr, C., Kangasluoma, J., Bianchi, F., Sun, Y., Croteau, P. L., Worsnop, D. R., Kerminen, V.-M., Du, W., Kulmala, M., and Daellenbach, K. R.: Size-segregated particle number and mass concentrations from different emission sources in urban Beijing, Atmos. Chem. Phys., 20, 12721–12740, https://doi.org/10.5194/acp-20-12721-2020, 2020.

Dinar, E., Mentel, T. F., and Rudich, Y.: The density of humic acids and humic like substances (HULIS) from fresh and aged wood burning and pollution aerosol particles, Atmos. Chem. Phys., 6, 5213–5224, doi:10.5194/acp-6-5213-2006, 2006.

Dameto de España, C., Wonaschütz, A., Steiner, G., Rosati, B., Demattio, A., Schuh, H., and Hitzenberger, R.: Long-term quantitative field study of New Particle Formation (NPF) events as a source of Cloud Condensation Nuclei (CCN) in the urban background of Vienna, Atmos. Environ., 164, 289–298, https://doi.org/10.1016/j.atmosenv.2017.06.001, 2017.

Flanner, M. G., Zender, C. S., Randerson, J. T., and Rasch, P. J.: Present-day climate forcing and response from black carbon in snow, J. Geophys. Res.-Atmos., 112, D11202, https://doi.org/10.1029/2006JD008003, 2007.

Fan, X., Liu, J., Zhang, F., Chen, L., Conllins, D., Xu, W., Jin, X., Ren, J., Wang, Y.,Wu, H., Li, S., Sun, Y., Li, Z.: Contrasting size-resolved hygroscopicity of fine particles derived by HTDMA and HR-ToF-AMS measurements between summer and winter in Beijing: the impacts of aerosol aging and local emissions, Atmos. Chem. Phys. 20, 915-929, https://doi.org/10.5194/acp-20-915-2020, 2020.

Geller, M., Biswas, S., and Sioutas, C.: Determination of particle effective density in urban environments with a differential mobility analyzer and aerosol particle mass analyzer, Aerosol Sci. Technol., 40, 709–723, https://doi.org/10.1080/02786820600803925, 2006.

Gysel, M., McFiggans, G. B., and Coe, H.: Inversion of tandem differential mobility analyser (TDMA) measurements, J. Aerosol Sci., 40, 134–151, https://doi.org/10.1016/j.jaerosci.2008.07.013, 2009.

Gysel, M., Crosier, J., Topping, D. O., Whitehead, J. D., Bower, K. N., Cubison, M. J., Williams, P. I., Flynn, M. J., McFiggans, G. B., and Coe, H.: Closure study between chemical composition and hygroscopic growth of aerosol particles during TORCH2, Atmos. Chem. Phys., 7, 6131–6144, https://doi.org/10.5194/acp-7-6131-2007, 2007.

Gunthe, S. S., King, S. M., Rose, D., Chen, Q., Roldin, P., Farmer, D. K., Jimenez, J. L., Artaxo, P., Andreae, M. O., Martin, S. T., and Pöschl, U.: Cloud condensation nuclei in pristine tropical rainforest air of Amazonia: size resolved measurements and modeling of atmospheric aerosol composition and CCN activity, Atmos. Chem. Phys.,

9, 7551–7575, https://doi.org/10.5194/acp-9-7551-2009, 2009.

Gysel, M., Laborde, M., Olfert, J. S., Subramanian, R., & Gröhn, A. J.: Effective density of aquadag and fullerene soot black carbon reference materials used for SP2 calibration, Atmos. Meas. Tech., 4(12), 4937–4955, https://doi.org/10.5194/amt-4-2851-2011, 2011.

Gysel, M., Laborde, M., Mensah, A. A., Corbin, J. C., Keller, A., Kim, J., et al.: Technical note: The single particle soot photometer fails to reliably detect PALAS soot nanoparticles, Atmos. Meas. Tech., 5(12), 3099–3107, https://doi.org/10.5194/amt-5-3099-2012, 2012.

Jimenez, J. L., Canagaratna, M. R., Donahue, N. M., Prevot, A. S. H., Zhang, Q., Kroll, J. H., DeCarlo, P. F., Allan, J. D., Coe, H., Ng, N. L., Aiken, A. C., Docherty, K. S., Ulbrich, I. M., Grieshop, A. P., Robinson, A. L., Duplissy, J., Smith, J. D., Wilson, K. R., Lanz, V. A., Hueglin, C., Sun, Y. L., Tian, J., Laaksonen, A., Raatikainen, T., Rautiainen, J., Vaattovaara, P., Ehn, M., Kulmala, M., Tomlinson, J. M., Collins, D. R., Cubison, M. J., Dunlea, E. J., Huffman, J. A., Onasch, T. B., Alfarra, M. R., Williams, P. I., Bower, K., Kondo, Y., Schneider, J., Drewnick, F., Borrmann, S., Weimer, S., Demerjian, K., Salcedo, D., Cottrell, L., Griffin, R., Takami, A., Miyoshi, T., Hatakeyama, S., Shimono, A., Sun, J. Y., Zhang, Y. M., Dzepina, K., Kimmel, J. R., Sueper, D., Jayne, J. T., Herndon, S. C., Trimborn, A. M., Williams, L. R., Wood, E. C., Middlebrook, A. M., Kolb, C. E., Baltensperger, U., and Worsnop, D. R.: Evolution of Organic Aerosols in the Atmosphere, Science., 326, 1525–1529, https://doi.org/10.1126/science.1180353, 2009.

Kiselev, A., Wennrich, C., Stratmann, F., Wex, H., Henning, S., Mentel, T.F., Kiendler-Scharr, A., Schneider, J., Walter, S., Lieberwirth, I.: Morphological characterization of soot aerosol particles during LACIS Experiment in November (LExNo), J. Geophys. Res. -Atmos., 115, D11204. https://doi.org/10.1029/2009jd012635, 2010.

Khalizov, A. F., Zhang, R., Zhang, D., Xue, H., Pagels, J., and McMurry, P. H.: Formation of highly hygroscopic soot aerosols upon internal mixing with sulfuric acid vapor, J. Geophys. Res.-Atmos., 114, D05208, https://doi.org/10.1029/2008jd010595, 2009.

Kawana, K., Nakayama, T., and Mochida, M.: Hygroscopicity and CCN activity of atmospheric aerosol particles and their relation to organics: Characteristics of urban aerosols in Nagoya, Japan, J. Geophys. Res.-Atmos., 121, 4100–4121, https://doi.org/10.1002/2015JD023213, 2016.

Kostenidou, E., Pathak, R. K., & Pandis, S. N.: An Algorithm for the Calculation of Secondary Organic Aerosol Density Combining AMS and SMPS Data, Aerosol Science and Technology, 41:11, 1002-1010, https://doi: 10.1080/02786820701666270, 2007.

Li, M., Zhang, Q., Kurokawa, J.-I., Woo, J.-H., He, K., Lu, Z., Ohara, T., Song, Y., Streets, D. G., Carmichael, G. R., Cheng, Y., Hong, C., Huo, H., Jiang, X., Kang, S., Liu, F., Su, H., and Zheng, B.: MIX: a mosaic Asian anthropogenic emission inventory under the international collaboration framework of the MICS-Asia and HTAP, Atmos. Chem. Phys., 17, 935–963, https://doi.org/10.5194/acp-17-935-2017, 2017.

Liu, D., Joshi, R., Wang, J., Yu, C., Allan, J. D., Coe, H., Flynn, M. J., Xie, C., Lee, J., Squires, F., Kotthaus, S., Grimmond, S., Ge, X., Sun, Y., and Fu, P.: Contrasting physical properties of black carbon in urban Beijing between winter and summer, Atmos. Chem. Phys., 19, 6749–6769, https://doi.org/10.5194/acp-19-6749-2019, 2019a.

Liu, D., Allan, J., Whitehead, J., Young, D., Flynn, M., Coe, H., McFiggans, G., Fleming, Z. L., and Bandy, B.: Ambient black carbon particle hygroscopic properties controlled by mixing state and composition, Atmos. Chem. Phys., *13*, 2015–2029, https://doi.org/10.5194/acp-13-2015-2013, 2013.

Liu, H., Pan, X.L., Wu, Y., Wang, D.W., Tian, Y., Liu, X.Y., et al.: Effective densities of soot particles and their relationships with the mixing state at an urban site in the Beijing megacity in the winter of 2018, Atmos. Chem. Phys. 19, 14791–14804, https://doi.org/10.5194/acp-19-14791-2019, 2019b.

Lide, D. R. (ed.). CRC Handbook of Chemistry and Physics. CRC Press: Ann Arbor, MI. (1992).

Lance, S., Medina, J., Smith, J., and Nenes, A.: Mapping the operation of the DMT continuous flow CCN counter, Aerosol Sci. Tech., 40, 242–254, https://doi.org/10.1080/02786820500543290, 2006.

Liu, H., Pan, X., Liu, D., Liu, X., Chen, X., Tian, Y., Sun, Y., Fu, P., and Wang, Z.: Mixing characteristics of refractory black carbon aerosols at an urban site in Beijing, Atmos. Chem. Phys., 20, 5771–5785, https://doi.org/10.5194/acp-20-5771-2020, 2020.

Liu, L, Zhang, J, Zhang, Y, Wang, Y, Xu, L, Yuan, Q, et al.: Persistent residential burning-related primary organic particles during wintertime hazes in North China: insights into their aging and optical changes, Atmos. Chem. Phys. *21,* 2251–2265, https://doi.org/10.5194/acp-21-2251-2021, 2021a.

Liu, J., Zhang, F., Xu, W., Sun, Y., Chen, L., Li, S.: Hygroscopicity of organic aerosols linked to formation mechanisms, Geophysical Research Letters, 48, e2020GL091683, https://doi.org/10.1029/2020gl091683, 2021b.

McMurry, H. Peter, Wang Xin, Park Kihong & Ehara Kensei.: The Relationship between Mass and Mobility for Atmospheric Particles: A New Technique for Measuring Particle Density, Aerosol Sci. Technol., 36:2, 227-238, https://doi.10.1080/027868202753504083, 2002.

Massoli, P., Onasch, T.B., Cappa, C.D., Nuamaan, I., Hakala, J., Hayden, K., Li, S.M., Sueper, D.T., Bates, T.S., Quinn, P.K., Jayne, J.T., Worsnop, D.R.: Characterization of black carbon-containing particles from soot particle aerosol mass spectrometer measurements on the R/V Atlantis during CalNex 2010, J. Geophys. Res.- Atmos., 120, 2575-2593, https://doi.org/10.1002/2014JD022834, 2015.

Mei, F., Setyan, A., Zhang, Q., and Wang, J.: CCN activity of organic aerosols observed downwind of urban emissions during CARES, Atmos. Chem. Phys., 13, 12155–12169, https://doi.org/10.5194/acp-13-12155-2013, 2013.

Meng, J. W., Yeung, M. C., Li, Y. J., Lee, B. Y. L., and Chan, C. K.: Size-resolved cloud condensation nuclei (CCN) activity and closure analysis at the HKUST Supersite in Hong Kong, Atmos. Chem. Phys., 14, 10267–10282, https://doi.org/10.5194/acp-14-

728   10267-2014, 2014.

729   McMeeking, G.R., Hamburger, T., Liu, D., Flynn, M., Morgan, W.T., Northway, M.,
730   Highwood, E.J., Krejci, R., Allan, J.D., Minikin, A., Coe, H.: Black carbon
731   measurements in the boundary layer over western and northern Europe. Atmos.
732   Chem. Phys. 10, 9393-9414, https://doi.org/10.5194/acp-10-9393-2010, 2010.

733   Noureddini, H., Teoh, B. C., Davis Clements, L.: Densities of vegetable oils and fatty

734   acids, J. Am. Oil Chem. Soc., 69 (12), 1184−1188, 1992.

735   Olfert, J. S., Symonds, J. P. R., and Collings, N.: The effective density and fractal
736   dimension of particles emitted from a light-duty diesel vehicle with a diesel oxidation
737   catalyst, J. Aerosol Sci., 38, 69–82, https://doi.org/10.1016/j.jaerosci.2006.10.002,
738   2007.

739   Park, K., Kittelson, D. B., and McMurry, P. H.: Structural properties of diesel exhaust
740   particles measured by transmission electron microscopy (TEM): Relationships to
741   particle   mass   and   mobility,   Aerosol   Sci.   Technol.,   38,   881–889,
742   https://doi.org/10.1080/027868290505189, 2004.

743   Pagels, J., Khalizov, A.F., McMurry, P.H. and Zhang, R.Y.: Processing of soot by
744   controlled sulphuric acid and water condensation-mass and mobility relationship,
745   Aerosol Sci. Technol., 43, 629–640, https://doi.org/10.1080/02786820902810685,
746   2009.

747   Peng, J. F., Hu, M., Guo, S., Du, Z. F., Zheng, J., Shang, D. J., Zamora, M., Zeng, L.
748   M., Shao, M., Wu, Y. S., Zheng, J., Wang, Y., Glen, C., Collins, D., Molina, M., and
749   Zhang, R. Y.: Markedly enhanced absorption, and direct radiative forcing of black
750   carbon under polluted urban environments, P. Natl. Acad. Sci. USA, 113(16), 4266–
751   4271, https://doi.org/10.1073/pnas.1602310113, 2016.

752   Petters, M. D. and Kreidenweis, S. M.: A single parameter representation of
753   hygroscopic growth and cloud condensation nucleus activity, Atmos. Chem. Phys.,
754   7, 1961–1971, https://doi.org/10.5194/acp-7-1961-2007, 2007.

755   Paatero, P. and Tapper, U.: Positive matrix factorization: A nonnegative factormodel
756   with optimal utilization of error estimates of data values, Environmetrics, 5, 111–126,
757   1994.

758   Peng, J. F., Hu, M., Guo, S., Du, Z. F., Zheng, J., M., Zeng, L. M., Shao, M., Wu, Y. S.,
759   Collins, D., Molina, M., and Zhang, R. Y.: Ageing and hygroscopicity variation of
760   black carbon particles in Beijing measured by a quasi-atmospheric aerosol evolution
761   study   (QUALITY)   chamber,   Atmos.   Chem.   Phys.,   17(17),   10333-10348,
762   https://doi.org/10.5194/acp-17-10333-2017, 2017.

763   Pan, X.L., Kanaya, Y., Taketani, F., Miyakawa, T., Inomata, S., Komazaki, Y., et al.:
764   Emission characteristics of refractory black carbon aerosols from fresh biomass
765   burning: a perspective from laboratory experiments, Atmos. Chem. Phys., 17(21),
766   13001–13016, https://doi.org/10.5194/acp-17-13001-2017, 2017.

767   Park, K., Cao, F., Kittelson, D. B., & McMurry, P. H.: Relationship between particle
768   mass and mobility for diesel exhaust particles, Environ. Sci. Tehnol., 37, 577–583,
769   https://doi.org/10.1021/es025960v, 2003.

770   Pileci, R. E., Modini, R. L., Bertò, M., Yuan, J., Corbin, J. C., Marinoni, A., Henzing,

B., Moerman, M. M., Putaud, J. P., Spindler, G., Wehner, B., Müller, T., Tuch, T., Trentini, A., Zanatta, M., Baltensperger, U., and Gysel-Beer, M.: Comparison of co-located refractory black carbon (rBC) and elemental carbon (EC) mass concentration measurements during field campaigns at several European sites, Atmos. Meas. Tech., 14, 1379–1403, https://doi.org/10.5194/amt-14-1379-2021, 2021.

Qiao, K., Wu, Z., Pei, X., Liu, Q., Shang, D., Zheng, J., Du, Z., Zhu,W.,Wu, Y., Lou, S., Guo, S., Chan, C.K., Pathak, R.K., Hallquist, M., Hu, M.: Size-resolved effective density of submicron particles during summertime in the rural atmosphere of Beijing. China, J. Environ. Sci. (China) 73, 69–77. https://doi.org/10.1016/j.jes.2018.01.012, 2018.

Rissler, J., Nordin, E. Z., Eriksson, A. C., Nilsson, P. T., Frosch, M., Sporre, M. K., Wierzbicka, A., Svenningsson, B., Londahl, J., Messing, M. E., Sjogren, S., Hemmingsen, J. G., Loft, S., Pagels, J. H., and Swietlicki, E.: Effective Density and Mixing State of Aerosol Particles in a Near-Traffic Urban Environment, Environ. Sci. Technol., 48, 6300–6308, https://doi.org/10.1021/es5000353, 2014.

Riemer, N., Vogel, H., and Vogel, B.: Soot aging time scales in polluted regions during day and night, Atmos. Chem. Phys., 4, 1885–1893, https://doi.org/10.5194/acp-4-1885-2004, 2004.

Ramanathan, V. and Carmichael, G.: Global and regional climate changes due to black carbon, Nat. Geosci., 36, 221-227, https://doi.org/10.1038/ngeo156, 2008.

Ren, J., Zhang, F., Wang, Y., Collins, D., Fan, X., Jin, X., et al.: Using different assumptions of aerosol mixing state and chemical composition to predict CCN concentrations based on field measurements in urban Beijing, Atmos. Chem. Phys., 18, 6907–6921, https://doi.org/10.5194/acp-18-6907-2018, 2018.

Rader, D.J., McMurry, P.H.: Application of the tandem differential mobility analyzer to studies of droplet growth or evaporation, J. Geophys. Res.- Atmos., 17, 771-787, https://doi.org/10.1016/0021-8502(86)90031-5, 1986.

Reyes-Villegas, E., Bannan, T., Le Breton, M., Mehra, A., Priestley, M., Percival, C., Coe, H., and Allan, J. D.: Online Chemical Characterization of Food-Cooking Organic Aerosols: Implications for Source Apportionment, Environ. Sci. Technol., 52, 5308–5318, https://doi.org/10.1021/acs.est.7b06278, 2018.

Schwarz, J.P., Gao, R.S., Fahey, D.W., Thomson, D.S., Watts, L.A., Wilson, J.C., Reeves, J.M., Darbeheshti, M., Baumgardner, D.G., Kok, G.L., Chung, S.H., Schulz, M., Hendricks, J., Lauer, A., K€archer, B., Slowik, J.G., Rosenlof, K.H., Thompson, T.L., Langford, A.O., Loewenstein, M., Aikin, K.C.: Single-particle measurements of midlatitude black carbon and light-scattering aerosols from the boundary layer to the lower stratosphere. J. Geophys. Res.: Atmosphere 111, D16207, https://doi.org/10.1029/2006JD007076, 2006.

Schwarz, J. P., Gao, R. S., Spackman, J. R., Watts, L. A., Thomson, D. S., Fahey, D. W., Ryerson, T. B., Peischl, J., Holloway, J. S., Trainer, M., Frost, G. J., Baynard, T., Lack, D. A., de Gouw, J. A., Warneke, C., and Del Negro, L. A.: Measurement of the mixing state, mass, and optical size of individual black carbon particles in urban and biomass burning emissions, Geophys. Res. Lett., 35, L13810, https://doi.org/10.1029/2008GL033968, 2008.

Stokes, R. and Robinson, R.: Interactions in aqueous nonelectrolyte solutions, I. Solute-solvent equilibria, J. Phys. Chem.-US, 70, 2126–2131, 1966.

Sun, Y., Du, W., Fu, P., Wang, Q., Li, J., Ge, X., Zhang, Q., Zhu, C., Ren, L., Xu, W., Zhao, J., Han, T., Worsnop, D. R., and Wang, Z.: Primary, and secondary aerosols in Beijing in winter: sources, variations, and processes, Atmos. Chem. Phys., 16, 8309–8329, https://doi.org/10.5194/acp-16-8309-2016,2016.

Sun, Y. L., Wang, Z. F., Du, W., Zhang, Q., Wang, Q. Q., Fu, P. Q., Pan, X. L., Li, J., Jayne, J., and Worsnop, D. R.: Long term real-time measurements of aerosol particle composition in Beijing, China: seasonal variations, meteorological effects, and source analysis, Atmos. Chem. Phys., 15, 10149–10165, https://doi.org/10.5194/acp-15-10149-2015, 2015.

Shiraiwa, M., Kondo, Y., Moteki, N., Takegawa, N., Sahu, L., Takami, A., et al.: Radiative impact of mixing state of black carbon aerosol in Asian outflow, J. Geophys. Res.- Atmos., 113, D24210, https://doi.org/ 10.1029/2008JD010546, 2008.

Tan, H., Xu, H., Wan, Q., Li, F., Deng, X., Chan, P. W., Xia, D., and Yin, Y.: Design and application of an unattended multifunctional H-TDMA system, J. Atmos. Ocean. Tech., 30, 1136–1148, https://doi.org/10.1175/JTECH-D-12-00129.1, 2013.

Ulbrich, I. M., Canagaratna, M. R., Zhang, Q., Worsnop, D. R., and Jimenez, J. L.: Interpretation of organic components from Positive Matrix Factorization of aerosol mass spectrometric data, Atmos. Chem. Phys., 9, 2891–2918, https://doi.org/10.5194/acp-9- 2891-2009, 2009.

Wang, Y., Wan, Q., Meng, W., Liao, F., Tan, H., and Zhang, R.: Long-term impacts of aerosols on precipitation and lightning over the Pearl River Delta megacity area in China, Atmos. Chem. Phys., 11, 12421–12436, https://doi.org/10.5194/acp-11-12421-2011, 2011.

Wang, Y. Y., Liu, F. S., He, C. L., Bi, L., Cheng, T. H., Wang, Z. L., Zhang, H., Zhang, X. Y., Shi, Z. B., and Li, W. J.: Fractal dimensions and mixing structures of soot particles during atmospheric processing, Environ. Sci. Tech. Lett., 4, 487–493, https://doi.org/10.1021/acs.estlett.7b00418, 2017.

Wu, Y. F., Xia, Y. J., Huang, R. J., Deng, Z. Z., Tian, P., Xia, X. G., et al.: A study of the morphology and effective density of externally mixed black carbon aerosols in ambient air using a size-resolved single-particle soot photometer (SP2), Atmos. Meas. Tech., 12, 4347–4359, https://doi.org/10.5194/amt-12-4347-2019, 2019.

Wu, Y., Wang, X., Tao, J., Huang, R., Tian, P., Cao, J., Zhang, L., Ho, K.-F., Han, Z., and Zhang, R.: Size distribution and source of black carbon aerosol in urban Beijing during winter haze episodes, Atmos. Chem. Phys., 17, 7965–7975, https://doi.org/10.5194/acp-17-7965-2017, 2017.

Wu, Z. J., Zheng, J., Shang, D. J., Du, Z. F., Wu, Y. S., Zeng, L. M., Wiedensohler, A., and Hu, M.: Particle hygroscopicity and its link to chemical composition in the urban atmosphere of Beijing, China, during summertime, Atmos. Chem. Phys., 16, 1123–1138, https://doi.org/10.5194/acp-16-1123-2016, 2016.

Xue, H., Khalizov, A. F., Wang, L., Zheng, J., and Zhang, R.: Effects of dicarboxylic acid coating on the optical properties of soot, Phys. Chem. Chem. Phys., 11, 7869–7875, https://doi.org/10.1039/b904129j, 2009.

Xu, W., Sun, Y., Wang, Q., Zhao, J., Wang, J., Ge, X., et al.: Changes in aerosol chemistry from 2014 to 2016 in winter in beijing: Insights from high-resolution aerosol mass spectrometry, J. Geophys. Res.-Atmos., 124, 1132–1147. https://doi.org/10.1029/2018jd029245, 2019.

Xu, W., Fossum, K. N., Ovadnevaite, J., Lin, C., Huang, R.-J., O'Dowd, C., and Ceburnis, D.: The impact of aerosol size-dependent hygroscopicity and mixing state on the cloud condensation nuclei potential over the north-east Atlantic, Atmos. Chem. Phys., 21, 8655–8675, https://doi.org/10.5194/acp-21-8655-2021, 2021.

Yuan, T., Li, Z., Zhang, R., and Fan, J.: Increase of cloud droplet size with aerosol optical depth: An observation and modeling study, J. Geophys. Res.-Atmos., 113, D04201, https://doi.org/10.1029/2007JD008632, 2008.

Yu, C., Liu, D., Broda, K., Joshi, R., Olfert, J., Sun, Y., Fu, P., Coe, H., Allan, J.D.: Characterising mass-resolved mixing state of black carbon in Beijing using a morphology-independent measurement method, Atmos. Chem. Phys., 20, 3645–3661. https://doi.org/10.5194/acp-20-3645-2020, 2020.

Zhang, R. Y., Khalizov, A. F., Pagels, J., Zhang, D., Xue, H. X., and McMurry, P. H.: Variability in morphology, hygroscopicity, and optical properties of soot aerosols during atmospheric processing, P. Natl. Acad. Sci. USA, 105, 10291–10296, https://doi.org/10.1073/pnas.0804860105, 2008.

Zhang, Y., Zhang, Q., Cheng, Y., Su, H., Kecorius, S., Wang, Z., Wu, Z., Hu, M., Zhu, T., Wiedensohler, A., and He, K.: Measuring the morphology and density of internally mixed black carbon with SP2 and VTDMA: new insight into the absorption enhancement of black carbon in the atmosphere, Atmos. Meas. Tech., 9, 1833–1843, https://doi.org/10.5194/amt-9-1833-2016, 2016.

Zdanovskii, A.: New methods for calculating solubilities of electrolytes in multicomponent systems, Zh. Fiz. Khim.C, 22, 1475– 1485, 1948.

Zhang, F., Wang, Y., Peng, J., Ren, J., Collins, D., Zhang, R., et al.: Uncertainty in predicting CCN activity of aged and primary aerosols, J. Geophys. Res.-Atmos., 122(21), 11723–11736, https://doi.org/10.1002/2017jd027058, 2017.

Zhang, F., Ren, J., Fan, T., Chen, L., Xu, W., Sun, Y., et al.: Significantly enhanced aerosol CCN activity and number, J. Geophys. Res.-Atmos., 124, 14102–14113, https://doi.org/10.1029/2019jd031457, 2019.

Zhang, F., Wang, Y., Peng, J., Chen, L., Sun, Y., Duan, L., Ge, X., Li, Y., Zhao, J., Liu, C., Zhang, X., Zhang, G., Pan, Y., Wang, Y., Zhang, A. L., Ji, Y., Wang, G., Hu, M., Molina, M. J., Zhang, R.: An unexpected catalyst dominates formation and radiative forcing of regional haze, P. Natl. Acad. Sci. USA, 117(8), 3960-3966, https://doi.org/10.1073/pnas.1919343117, 2020a.

Zhang, Y., Zhang, Q., Yao, Z., Li, H.: Particle Size and Mixing State of Freshly Emitted Black Carbon from Different Combustion Sources in China, Environ. Sci. Technol., 54(13): p. 7766-7774, https://doi.org/10.1021/acs.est.9b07373, 2020b.

Zhang, F., Peng, J., Chen, L., Collins, D., Li, Y., Jiang, S., Liu, J., Zhang, R.: The effect of Black carbon aging from NO2 oxidation of SO2 on its morphology, optical and hygroscopic properties, Environ. Res., 212, 113238, https://doi.org/10.1016/j.envres.2022.113238, 2022.

Zhang, R., Wang, G., Guo, S., Zamora, M. L., Ying, Q., Lin, Y.: Formation of urban fine particulate matter, Chemical Reviews, 115(10), 3803–3855, https://doi.org/10.1021/acs.chemrev.5b00067, 2015.

Zhou, Y., Ma, N., Wang, Q., Wang, Z., Chen, C., Tao, J., Hong, J., Peng, L., He, Y., Xie, L., Zhu, S., Zhang, Y., Li, G., Xu, W., et al.: Bimodal distribution of size-resolved particle effective density: results from a short campaign in a rural environ ment over the North China Plain, Atmos. Chem. Phys., 22, 2029–2047. https://doi.org/10.5194/acp-22-2029-2022, 2022.

Zhao, G., Tan, T., Hu, S., Du, Z., Shang, D., Wu, Z., Guo, S., Zheng, J., Zhu, W., Li, M., Zeng, L., and Hu, M.: Mixing state of black carbon at different atmospheres in north and southwest China, Atmos. Chem. Phys., 22, 10861–10873, https://doi.org/10.5194/acp-22-10861-2022, 2022.